47th AIAA Aerospace Sciences Meeting Including The New Horizons Forum and Aerospace Exposition
5 - 8 January 2009, Orlando, Florida

AIAA 2009-777

Optimization of Pulsed Jets in Crossflow

Rajes Sau* and Krishnan Mahesh†

University of Minnesota, Minneapolis, MN, 55414, USA

Recent experiments (M'Closkey et al. 2002, Shapiro et al. 2006, Johari 2006, Eroglu and Briedenthal 2001) on pulsed jets in crossflow show that jet penetration and spread can be optimized at specific pulse conditions. We perform DNS to study the evolution and mixing behavior of jets in crossflow at different velocity ratios with fully modulated square wave excitation. We attempt to explain the wide range of optimal pulsing conditions found in different experiments by noting that pulsing generates vortex rings. Sau and Mahesh (J. Fluid Mech., 2008) show that vortex rings in crossflow exhibit three distinct flow regimes depending on stroke ratio and ring velocity ratio. We use the behavior of a single vortex ring in crossflow to explain the evolution of pulsed jets in crossflow. Simulations suggest that the optimal conditions can be predicted from the transition behavior of vortex rings between different regimes. An optimal map in stroke ratio and velocity ratio space is presented and used to obtain an a-priori estimate of optimal conditions. Good comparison with different experimental optimal conditions are obtained in terms of stroke ratio and ring velocity ratio.

I. Introduction

Jets in crossflow have a wide range of important applications such as dilution holes in combustors, fuel injectors, pollutant dispersion from smoke stacks, thrust vectoring of turbojets, and V/STOL aircraft. Extensive research have been performed on jets in crossflow over the last few decades. Recently, there has been considerable attempt to control this three dimensional canonical flow. Recent experiments (e.g. Wu *et al.* 1988, Chang & Vakili 1995, Hermanson *et al.* 1998, Johari *et al.* 1999, Eroglu & Briedenthal 2001, Blossey *et al.* 2001, M'Closkey *et al.* 2002, Karagozian *et al.* 2003, Shapiro *et al.* 2006) have examined pulsing of the jet as a means of control. These experiments have attempted to optimize jet penetration, spread into the crossflow. It is shown that the jet can be optimized at specific pulsing conditions. But, the optimal pulsing conditions vary over a wide range; e.g. $St = 0.004$ to 0.5.

It can be observed in these experiments that the pulsing of the jet creates distinct vortex rings which play crucial role in penetration and mixing (Eroglu & Briedenthal 2001, M'Closkey *et al.* 2002, Shapiro *et al.* 2006). When the flow rate of the jet is periodically modulated by a square wave, distinct vortex rings are created whose spacing and strength is dictated by the pulsing frequency for a given jet and crossflow combination (Eroglu & Briedenthal 2001). M'Closkey *et al.* (2002) report that square wave excitation is more effective than the sinusoidal forcing as square wave excitation results in distinct vortex ring formation which penetrate deeply into the crossflow. The experiments of Johari *et al.* (1999) show that enhancement in penetration for fully pulsed jets with long injection time is moderate, whereas short injection time and smaller duty cycle produces vortex rings which results in significant enhancement over the steady jet. For fixed injection time, increasing the frequency results in lower penetration due to the increased interaction between the structures.

*Graduate Research Assistant
†Associate Professor

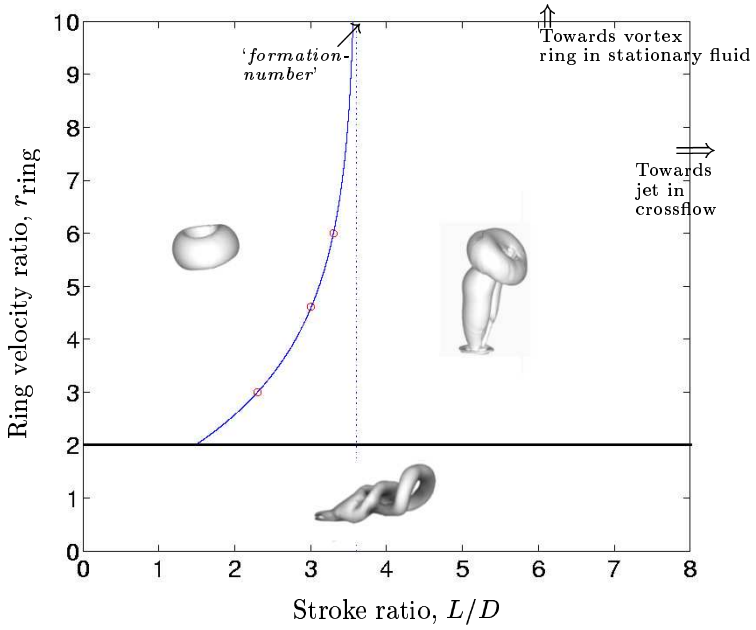

Figure 1. Classification map showing three regimes with different flow structure and entrainment characteristics of vortex rings in crossflow (Sau & Mahesh 2008).

M'Closkey *et al.* (2002) and Shapiro *et al.* (2003) relate optimal pulse width for maximum penetration to the universal time scale or 'formation number' of vortex ring formation proposed by Gharib *et al.* (1998). Interestingly, the critical stroke ratio, for deeply penetrating vortical structures and optimal jet penetration, is obtained roughly one-half of 'formation number'. The reason for obtaining much smaller stroke ratio than the 'formation number' is not clearly addressed. They argue that the timescales associated with the transverse jet may be coupled in a way that leads to these smaller stroke ratios. Again, the relation between optimal condition for penetration in crossflow and time scale of vortex ring formation is not examined previously. Johari (2006) presents scaling arguments for pulsed jet in crossflow based on the motions of vortex ring in stationary fluid, thus completely ignoring the effect of crossflow.

Although the experiments of pulsed jets in crossflow suggest that vortex rings play a key role, there have been very few experiments or simulations which examine the dynamics and mixing characteristics of vortex rings in the presence of crossflow. Sau & Mahesh (2007) use DNS to study optimal mixing by a single vortex ring in stationary fluid. They consider two Schmidt numbers and a range of stroke ratios. The formation number is found to yield the maximum entrainment for both Schmidt numbers. This study ignores the effect of crossflow. Sau & Mahesh (2008) perform DNS to study the effect of crossflow on vortex rings in detail. Three different regimes are found to exist depending on the stroke ratio and velocity ratio. A classification map is obtained which categorizes these three different regimes as shown in figure 1. For velocity ratio less than approximately 2, complete vortex ring structures do not form. Instead, a hairpin vortex forms at these low velocity ratios. For velocity ratios above 2, two regimes are obtained depending upon stroke ratio. Lower stroke ratios yield a vortex ring tilted upstream, while higher stroke ratios yield a downstream tilted vortex ring accompanied by a trailing column of vorticity. A transition curve in the map defines the transition from a discrete vortex ring to a vortex ring with trailing column. The transition stroke ratio decreases with decreasing velocity ratio. For very high values of velocity ratio, the transition stroke ratio approaches the 'formation number'.

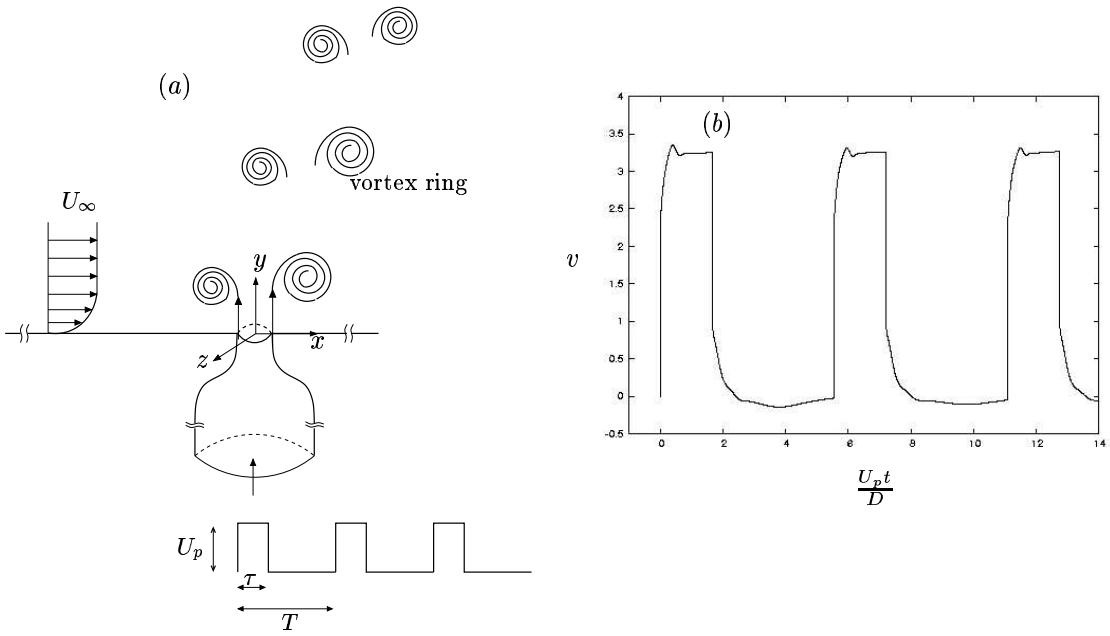

Figure 2. (a) A schematic of the problem. (b) A typical waveform at the nozzle exit resulting from a square waveform specified at the nozzle inflow.

The above study has important implications to pulsed jet in crossflow. The pulsing/forcing conditions of the jet can be transformed into the ring parameters (stroke ratio and velocity ratio) and can be mapped onto the classification map (figure 1). The map categorizes the complete space of velocity ratio and stroke ratio into specific regimes of flow structure. The transformed pulsing parameters in the classification map can be used to predict the flow structures *a-priori*. Desired flow feature can also be obtained by choosing the corresponding parameter from the map. The objective of this paper is to examine the optimal conditions for pulsed jets in crossflow using ideas developed for single vortex rings in crossflow. Controlled simulations of fully modulated pulsed jet in crossflow are performed for different pulsing parameters chosen judiciously from the classification map. It will be shown that the optimal penetration of the pulsed jet can be obtained and explained using the behavior of single vortex ring in crossflow. This paper also attempts to explain the optimal conditions observed in various experiments on pulsed jets in crossflow.

This paper is organized as follows. Section II discusses the problem and details of the simulations. Simulation results are presented in section IVA. Experimental results are analyzed and interpreted in section IVB. Conclusions are briefly discussed in section V.

II. Simulation details

Figure 2(a) shows a schematic of the problem, in which a fully modulated pulsed jet is injected through a cylindrical nozzle with 3 : 1 diameter ratio. As a result of pulsing, the nozzle fluid forms a series of vortex rings as it exits the nozzle. These vortex rings interact with the crossflow which is directed along the $x-$direction. The crossflow is modeled as a laminar boundary layer over a flat plate. The origin of the coordinate system is located at the center of the nozzle exit plane, and the nozzle axis points in the $y-$direction.

A square wave excitation is prescribed at the nozzle inflow to simulate a pulsed jet. Figure 2(b) shows the exit velocity waveform at the center of the nozzle exit plane for a particular pulsing condition. Note that the exit velocity waveform is very close to a square wave–form as prescribed. In experiments, the exit-velocity waveform is far from the prescribed inflow waveform due to the issues regarding pulsing and flow inside the

Table 1. Performed simulations and optimal conditions.

Vortex ring regime, $r_{\text{ring}} > 2$.				
Case	r_{ring}	Duty Cycle, α	Optimal St^*	Optimal $\frac{L}{D}^*$
1	8.0	30%	0.28	3.5
2		20%	0.28	3.5
3	6.0	20%	0.4	2.5
4	4.5	15%	0.5	2.0
5		20%	0.5	2.0
6		40%	No optimal	No optimal
7	3.5	20%	0.67	1.5

nozzle. For example, M'Closkey *et al.* (2002) used a linear compensator in their experiments in order to get a square waveform at nozzle-exit close to the prescribed waveform at inflow. In our present configuration, there is no need of such control strategy. As shown in the schematic, square pulses are excited at a particular frequency, f which is non–dimensionalized using the mean jet velocity $\overline{U}_j$ and the nozzle exit diameter D. The non–dimensional frequency is denoted by the Strouhal number $St = \frac{fD}{\overline{U}_j}$, where the mean jet velocity $\overline{U}_j$ is obtained by averaging nozzle exit velocity over the nozzle cross–section in one time period (T). Duty cycle, α is defined as the ratio of pulse width (τ) to the time period ($\alpha = \frac{\tau}{T}$). Pulse width is the time during which the pulse is 'on'. For fully modulated jet, the inflow velocity is set to zero when the pulse is 'off'. The peak pulse velocity is denoted as U_p. U_∞ is the free–stream crossflow velocity. The mean jet to crossflow velocity ratio r_j is defined as the ratio of mean jet velocity $\overline{U}_j$ to the free–stream crossflow velocity (U_∞). Reynolds number based on U_p and nozzle exit diameter (D) is 650.

Each time period or cycle of pulsing jet leads to a vortex ring. The relevant parameter for vortex ring formation is the stroke ratio, L/D (ratio of stroke length L to the nozzle exit diameter D). In experiments, vortex rings are generated by ejecting a column(L) of fluid though the nozzle(D) by short impulse. For pulsed jets, the equivalent stroke ratio, L/D of vortex ring formation can be related to pulsing parameters (e.g. St, α). For fully modulated square wave excitation, the relations are derived as follows. In each cycle, equivalent stroke length, $L = \Delta U_j \tau = U_p \tau = U_p \alpha T$. And the mean jet velocity, $\overline{U}_j = \frac{1}{T}\int_0^T u\ dt = U_p \alpha$. So, the stroke ratio,

$$\frac{L}{D} = \frac{\Delta U_j \tau}{D} = \frac{\Delta U_j \alpha}{fD} = \left(\frac{\Delta U_j \alpha}{\overline{U}_j}\right)\left(\frac{\overline{U}_j}{fD}\right) = \left(\frac{U_p \alpha}{\overline{U}_j}\right)\left(\frac{1}{St}\right)$$

This implies, for fully modulated square wave excitation,

$$\frac{L}{D} = \frac{1}{St}.$$

So, the equivalent stroke ratio of vortex ring formation is the inverse of the non-dimensional pulsing frequency. Due to the presence of crossflow, another important parameter is the ring velocity ratio, r_{ring} which is defined as the ratio of peak to peak pulse velocity ΔU_j to the free–stream crossflow velocity U_∞.

$$r_{\text{ring}} = \frac{\Delta U_j}{U_\infty} = \frac{U_p}{U_\infty}.$$

Table 1 lists the conditions for different cases of simulations performed. In each simulation, a square waveform is used with fixed U_p. Ring velocity ratio is varied by varying the free–stream crossflow velocity.

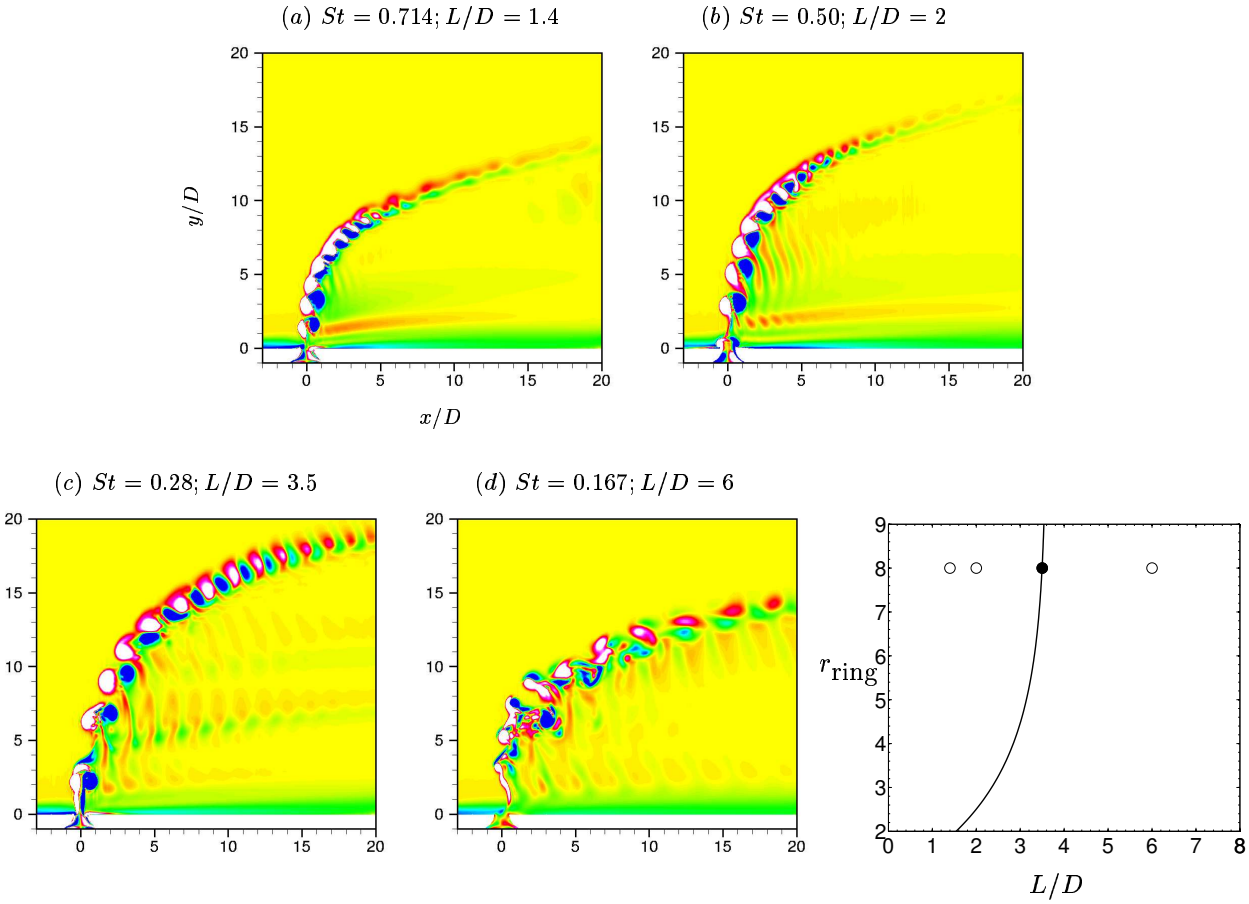

Figure 3. Case 1: Contours of z vorticity(fig. a–d) in symmetry plane. Ring velocity ratio, $r_{\mathbf{ring}} = 8.0$ and duty cycle, $\alpha = 30\%$ are fixed ($U_p = 3.0, U_\infty = 0.38$). Strouhal number is varied as (a) $St = 0.714$; (b) $St = 0.50$; (c) $St = 0.28$; (d) $St = 0.167$. Note that the maximum penetration is being achieved for $St = 0.28$ which corresponds to equivalent stroke ratio of 3.5. Different simulation conditions are marked in classification map (fig e). The solid symbol in fig (e) corresponds to $St = 0.28$ (fig c).

As detailed in table 1, Strouhal number (St) or equivalent stroke ratio (L/D) is varied to examine the optimal pulse conditions while keeping ring velocity ratio and duty cycle constant. So, for a given ring velocity ratio, mean jet to crossflow velocity ratio, r_j remains constant as St is being varied. St ranges from 2.0 to 0.167 which corresponds to the variation of L/D from 0.5 to 6. Table 1 also tabulates the optimal St and optimal L/D for different cases.

III. Numerical method

The numerical scheme solves the incompressible Navier Stokes and continuity equations

$$\frac{\partial u_i}{\partial t} + \frac{\partial u_i u_j}{\partial x_j} = -\frac{\partial p}{\partial x_i} + \nu \frac{\partial^2 u_i}{\partial x_j x_j} \quad , \quad \frac{\partial u_i}{\partial x_i} = 0 \tag{1}$$

on unstructured grids. Here u_i, p and ν denote the velocities, pressure and kinematic viscosity respectively. The density of the fluid is assumed constant and is absorbed into the pressure. The numerical scheme

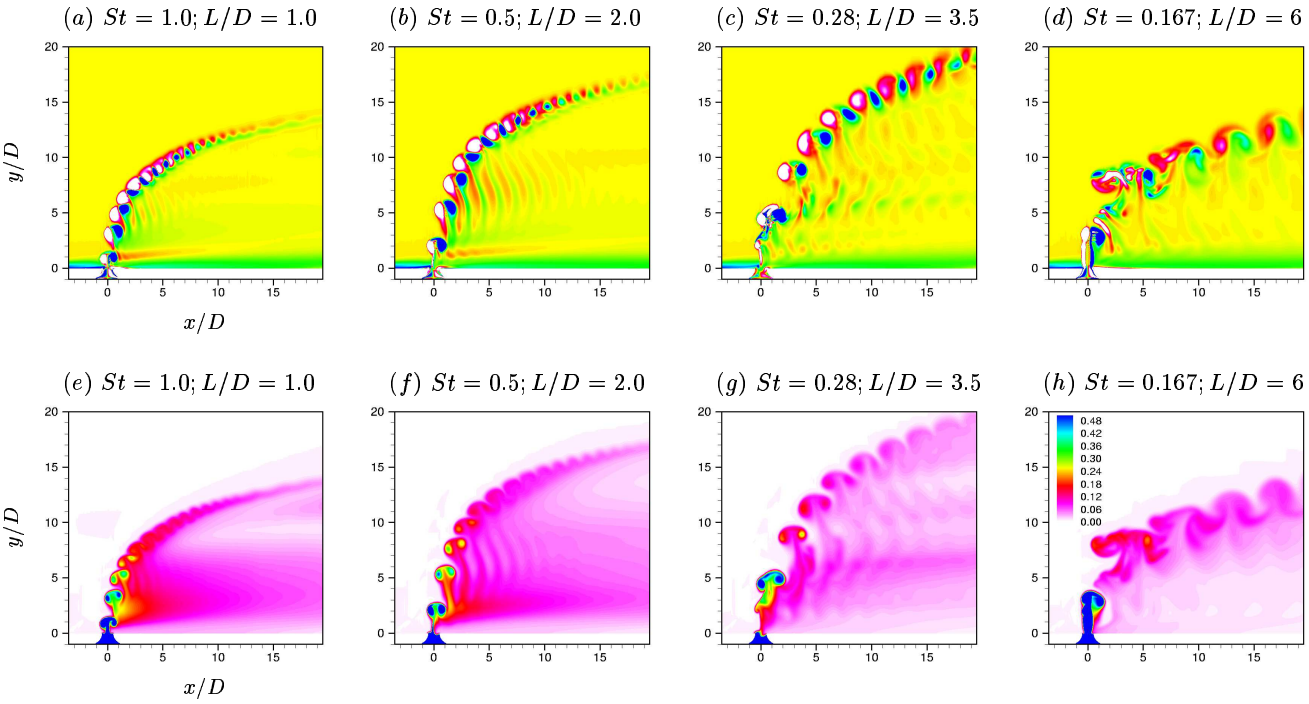

Figure 4. Case 2: Contours of z vorticity (fig. a–d) and scalar concentration (fig. e–h) in symmetry plane. Ring velocity ratio, $r_{\mathbf{ring}} = 8.0$ and duty cycle, $\alpha = 20\%$ are fixed ($U_p = 3.0, U_\infty = 0.38$). Strouhal number is varied as (a) $St = 0.714$; (b) $St = 0.50$; (c) $St = 0.28$; (d) $St = 0.167$. Note that the maximum penetration is being achieved for $St = 0.28$ which corresponds to equivalent stroke ratio of 3.5.

is described in detail by Mahesh, Constantinescu & Moin (2004). The algorithm stores the Cartesian velocities and the pressure at the centroids of the cells (control volumes) and the face normal velocities are stored independently at the centroids of the faces. The scheme is a predictor–corrector formulation which emphasizes discrete energy conservation on unstructured grids. This property makes the algorithm robust at high Reynolds numbers without numerical dissipation. The predicted velocities at the control volume centroids are obtained using the viscous and the non–linear terms of equation 1 which are then used to predict the face normal velocities on the faces. The predicted face normal velocity is projected so that continuity is discretely satisfied. This yields a Poisson equation for pressure which is solved iteratively using a multigrid approach. The pressure field is used to update the Cartesian control volume velocities. Implicit time–stepping is performed using a Crank–Nicholson scheme. The algorithm has been validated for a variety of problems over a range of Reynolds numbers (Mahesh *et al.* 2004).

IV. Results

A. Simulation results

Optimal pulsing conditions at different velocity ratios are examined. It will be shown here that the classification map (figure 1) for single vortex ring in crossflow (Sau & Mahesh 2008) can be used to predict the optimal conditions in pulsed jet in crossflow.

Figure 3 shows the simulation results for case 1. Contours of ω_z–vorticity are plotted in the symmetry plane. The ring velocity ratio ($r_{\text{ring}} = 8$) and duty cycle ($\alpha = 20\%$) are fixed as frequency or St is varied: (a) $St = 0.714$; (b) $St = 0.50$; (c) $St = 0.28$; (d) $St = 0.167$. The equivalent stroke ratios for these cases can

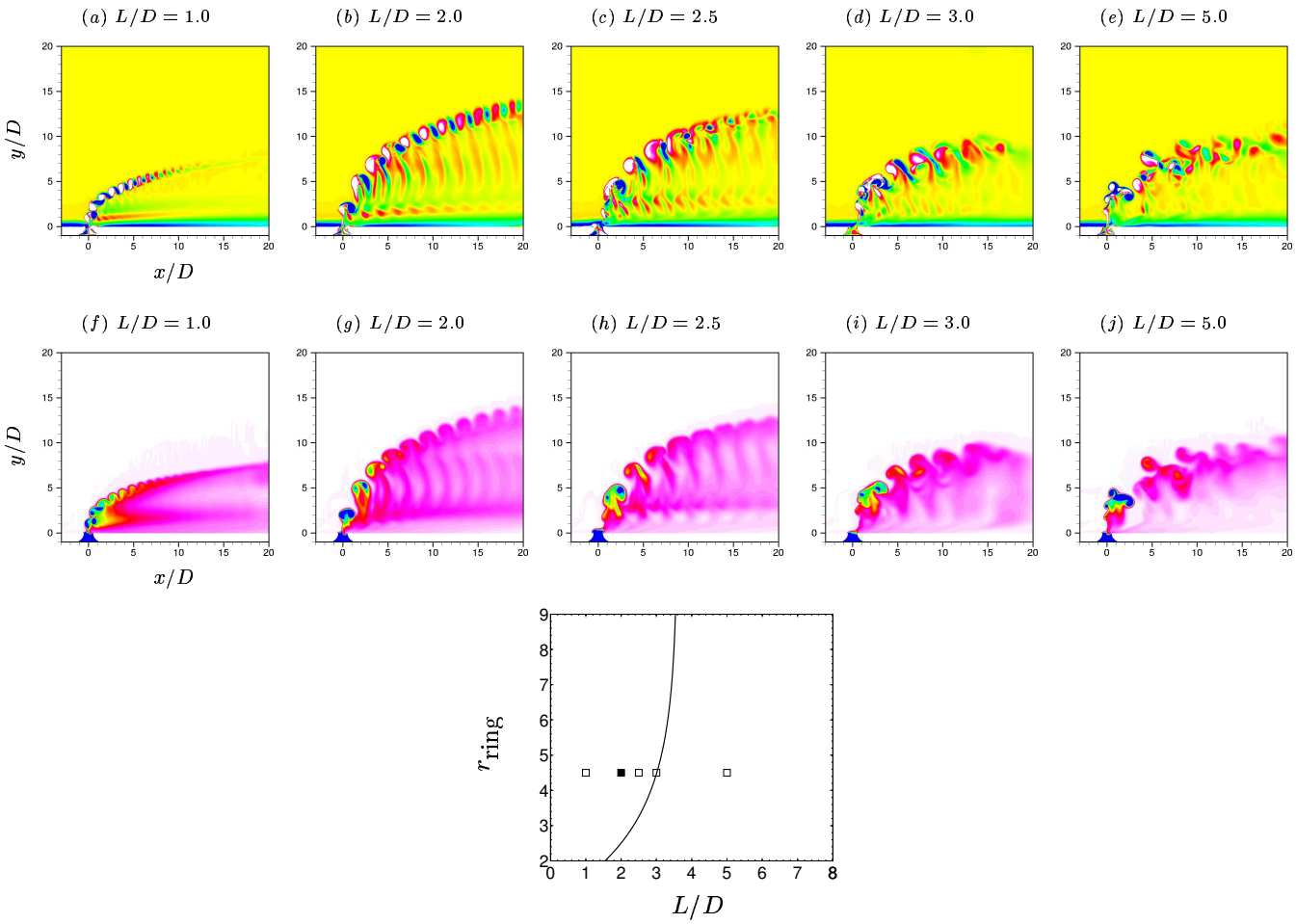

Figure 5. Case 5: Contours of z vorticity (fig. a–e) and scalar concentration (fig. f–j) in symmetry plane. Ring velocity ratio, $r_{\mathbf{ring}} = 4.5$ and duty cycle is at 20% ($U_p = 3.0, U_\infty = 0.67$). Strouhal number or Stroke ratio is varied as: (a) & (f) $St = 1.0, L/D = 1.0$; (b) & (g) $St = 0.5, L/D = 2.0$; (c) & (h) $St = 0.4, L/D = 2.5$; (d) & (i) $St = 0.333, L/D = 3.0$; (e) & (j) $St = 0.2, L/D = 5.0$. Note that the optimal penetration is obtained at $St = 0.5$ or equivalent stroke ratio of 2. Different conditions are marked in the classification map in figure (k).

be computed from St and are noted in figure 3. Note that the maximum penetration of the jet is obtained for $St = 0.28$ or $L/D = 3.5$ in figure 3(c). These results can readily be interpreted using the classification map (figure 1). The ring parameters, stroke ratio and ring velocity ratio, for these pulsing conditions are shown in the classification map in figure 3(e). The solid symbol corresponds to the optimal condition. Note that the optimal stroke ratio lies on the transition curve.

In figure 3(a)–(c), for $L/D \leq 3.5$ (or $St \geq 0.28$), the pulsed jet produces series of upstream tilted vortex rings without any trailing column of vorticity. Vortex rings with $L/D = 1.4$ and 2.0 (fig.3a & 3b respectively) contain much less circulation or momentum compared to rings of $L/D = 3.5$ (fig.3c) . Thus, the rings interact in the near field and the penetration is less. Whereas in figure 3(c), vortex rings (upstream tilted) contain maximum momentum as the L/D is about the transition stroke ratio at $r_{\text{ring}} = 8$ and penetrates deep into the crossflow before interacting or merging with each other. On the other hand, in figure 3(d) ($St = 0.167$), vortex rings along with trailing column of vorticity is produced as the stroke ratio, $L/D = 6$, is higher than the transition stroke ratio. These rings have approximately the same momentum as of $L/D = 3.5$ (figure 3c), but the rings tilt in the downstream direction and also have trailing columns which strongly interact

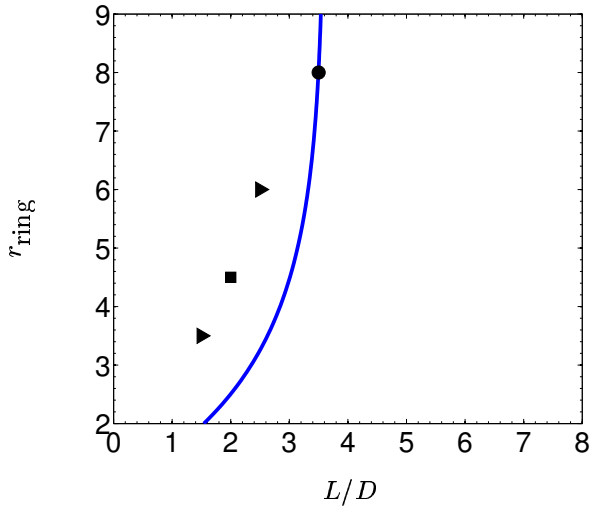

Figure 6. The optimal conditions are plotted in stroke ratio and ring velocity ratio space along with transition curve (classification map) for different simulation cases: ∘, case 1 & 2; ∇, case 3; □, case 4 & 5; △, case 7. The filled–symbols denote the optimal conditions (table 1) at given ring velocity ratios. The solid line denotes the transition curve.

with subsequent structure in the near field itself. This interaction does not allow deeper penetration into the crossflow. Thus the optimal penetration is obtained at $St = 0.28$ or $L/D = 3.5$ for $r_{\mathrm{ring}} = 8$.

Figure 4 shows the simulation results for case 2. In this case, conditions are similar to case 1 except duty cycle is lowered to 20%. Figures 4(a)–(d) show ω_z–vorticity contours and figures 4(e)–(h) show scalar contours in the symmtry plane. Note that varying the duty cycle does not alter the optimal condition. However, for large duty cycle, no optimal penetration is obtained since the rings interact in the very near field irrespective of pulsing frequency. Also, the trajectories are similar at different frequencies. This behavior is pronounced at lower ring velocity ratios as discussed later. Figures of passive scalar (fig. 4e–h) reveal an interesting structural feature of the pulsed jets. It can easily be observed (fig. 4e–g) that the jet splits in two streams at optimal stroke ratio and at stroke ratios lower than the optimal. For stroke ratio higher than the optimal no such splitting is observed (fig 4h). The multiple streams are observed in the case of single vortex ring generated regime and the second stream is formed by the wake of the rings being convected by the crossflow.

Next, the optimal conditions at lower ring velocity ratios are examined. Figure 5 shows the results for case 5 in table 1. The ring velocity ratio and duty cycle are fixed at 4.5 and 20% respectively. Figure 5(a)–(e) show the vorticity contours in the symmetry plane at different strouhal number or different stroke ratio. Note that the optimal penetration is obtained at $St = 0.5$ or $L/D = 2.0$ in figure 5(b). The simulations conditions are again mapped onto stroke ratio and ring velocity ratio space as shown in figure 5(k). The solid symbol corresponds to the optimal penetration condition. Note that optimal condition lies left of the transition curve. The reason for the left shift of optimal condition is because of the induced interaction among successive rings. Even at this low duty cycle of 20%, the interaction among successive ring is strong as the L/D approaches the transition curve. The effect of duty cycle is studied by varying the duty cycle and running other sets of simulations at the same $r_{\mathrm{ring}} = 4.5$ as shown in table 1 (case 4 and 6). For duty cycle of 15% (case 4), the same optimal condition is obtained. So, as already stated for $r_{\mathrm{ring}} = 8$, the opimal condition does not change as the duty cycle is lowered. Whereas, at 40% duty cycle, no optimal is found. So, as long as the duty cycle is low enough, optimal penetration is found to exist and variation of duty cycle only changes penetration difference between optimal and non–optimal cases.

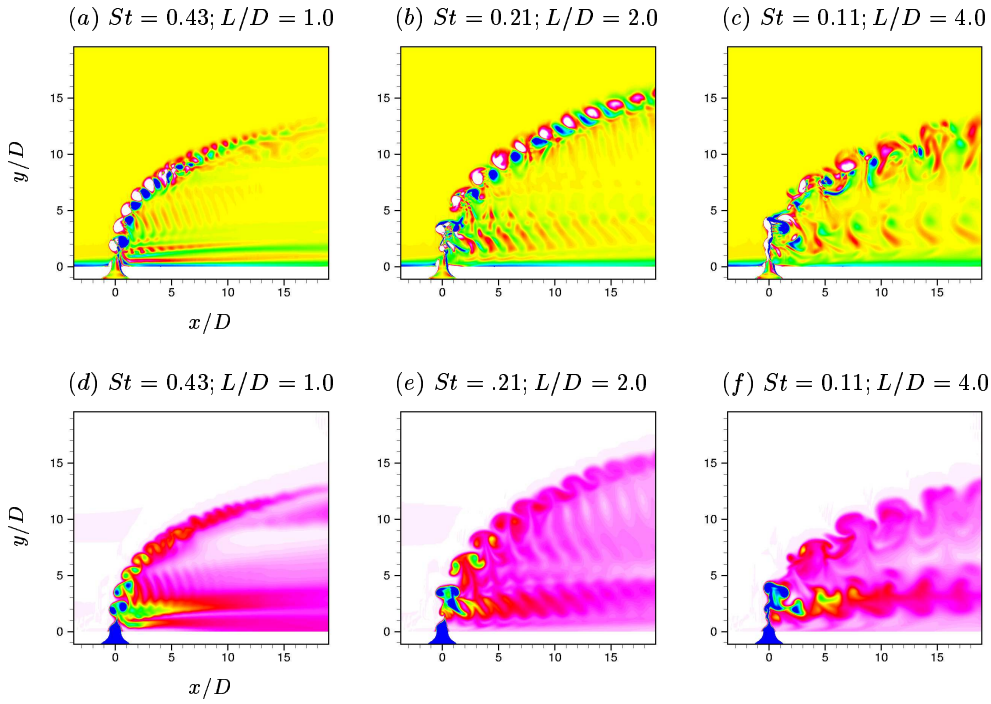

Figure 7. Partial modulation (75%): Contours of z vorticity (fig. a–c) and scalar concentration (fig. e–g) in symmetry plane. Ring velocity ratio, $r_{\mathbf{ring}} = 4.5$ and duty cycle is at 25% ($\overline{U}_j = 1.75, \Delta U = 3.0, U_\infty = 0.67$). Strouhal number or Stroke ratio is varied as: (a) & (d) $St = 0.43, L/D = 1.0$; (b) & (e) $St = 0.21, L/D = 2.0$; (c) & (f) $St = 0.11, L/D = 4$. Note that the optimal penetration is obtained at $St = 0.21$ or equivalent stroke ratio of 2 and $r_{\mathbf{ring}} = 4.5$.

In order to estimate the variation of optimal conditions as a function of velocity ratio, simulations are also performed at $r_{\text{ring}} = 6$ (case 3) and 3.5 (case 7) as listed in table 1. The optimal St or the equivalent stroke ratio L/D for optimal penetration is tabulated. Figure 6 shows the different optimal conditions obtained in the simulations. The symbols correspond to the equivalent stroke ratios for optimal penetration at different ring velocity ratios and the solid curve shows the transition curve. The optimal stroke ratio lies around the transition stroke ratio at high ring velocity ratio. Note that the optimal stroke ratio lies on the left of the transition curve for lower velocity ratios and decreases as the velocity ratio decreases. The transition curve represents the transition in structure and tilting for *single* vortex ring in crossflow. Figure 6 shows that the optimal stroke ratio at lower ring velocity ratios for pulsed jets (series of ring) is smaller than the transition stroke ratio found in the case of single vortex ring. As already mentioned, this is due to the effect of subsequent interaction between rings. A curve representing optimal stroke ratios at different velocity ratios can be estimated passing through the points shown in the figure. Therefore, this map along with the optimal points can be used to estimate or predict optimal conditions for pulsed jets in crossflow.

Partially modulated pulsed jets

All simulation cases discussed thus far consider pulsed jets with 100% modulation, where the minimum jet velocity during a time period is zero. In other words, percentage modulation is defined as the ratio of maximum jet velocity to the peak–to–peak jet velocity difference. The optimal values in figure 6 correspond to simulation cases with 100% modulation. Now, in the case of partial modulation, the equivalent stroke ratio of vortex ring formation and ring velocity ratio should be based on the peak–to–peak velocity difference

and crossflow free–stream velocity as defined in section II. So, the optimal conditions in terms of stroke ratio and ring velocity ratio in partially modulated jet would still be the same as fully modulated jet (figure 6) as long as the parameters are defined properly based on peak–to–peak velocity difference. In order to show this, an additional set of simulations are performed for 75% modulated jet at ring velocity ratio of 4.5 as shown in figure 7. Contours of z vorticity (fig 7a–c) and scalar concentration (fig 7d–f) are plotted in the symmetry plane. Strouhal number St is being varied (St = (a) 0.43, (b) 0.21 and (c) 0.11) while keeping the duty cycle (α = 25%) and ring velocity ratio (r_{ring} = 4.5) fixed. The corresponding stroke ratios are also noted in figure 7. As discussed in section II, $St = D/L$ for fully modulated square wave excitation. On the other hand, for partial modulation, the relation will involve the base flow. In this particular case, $St = 0.43 \times D/L$. Figure 7(b) shows the optimal penetration and corresponds to equivalent stroke ratio of 2. Note that it is already shown that the optimal stroke ratio is 2 at ring velocity ratio of 4.5. Thus, in the case of partial modulation, the optimal conditions can be predicted using the equivalent stroke ratio and ring velocity ratio as shown in figure 6.

Note that, in all the cases in figure 7(d–f), the scalar contours show multiple streams for the pulsed jet. Even in the case of vortex ring with trailing column (e.g. fig 7g, L/D = 4), the jet splits in two streams unlike the fully modulated jet. Due to the partial modulation, the minimum jet velocity is non–zero. So, the jet basically consists of high momentum fluid that generates rings and low momentum fluid that stays close to the wall. The second stream is mainly due to the non-zero jet velocity during the time when pulse is 'off'.

B. Interpretation and comparison of experimental results

An optimal map for pulsed jets in crossflow is being developed using controlled simulation and ideas from single vortex ring in crossflow. In this section, we interpret various experimental results on pulsed jets in crossflow using the optimal map. The optimal conditions found in different experiments vary a wide range. It will be shown here that different optimal conditions can be predicted or explained using the corresponding vortex ring parameters namely stroke ratio and ring-velocity ratio (classification map). We will compare the optimal parameters in experiments with our simulations in terms of optimal map. It will also be shown that particular flow features observed in some experiments of pulsed jet can be interpreted using the optimal map.

Table 2. Experimental Conditions of Shapiro *et al.* (2006).

Case	$\bar{U}_j$ m/s	U_∞	r_j	$U^{'}_{j,\text{rms}}$	Re_j	f	α or τ	τ_{opt} ms
1	2.8	1.1	2.58	1.5	1420	varied 44–147 Hz	varied 10–50%	3.0
4	7.2	1.8	4.0	2.3	3660	varied 87–130 Hz	varied 10–50%	1.6

Table 3. Case 1 of Shapiro *et al.*; optimal conditions ($U^{'}_{j,\text{rms}}$ is matched at 1.5 m/s)

Frequency Hz	Optimal τ	Optimal ring parameters	
		equivalent L/D^*	r_{ring}
44	3 ms	1.80	3.93
55		1.68	3.55
73.5		1.50	3.19
110		1.28	2.88

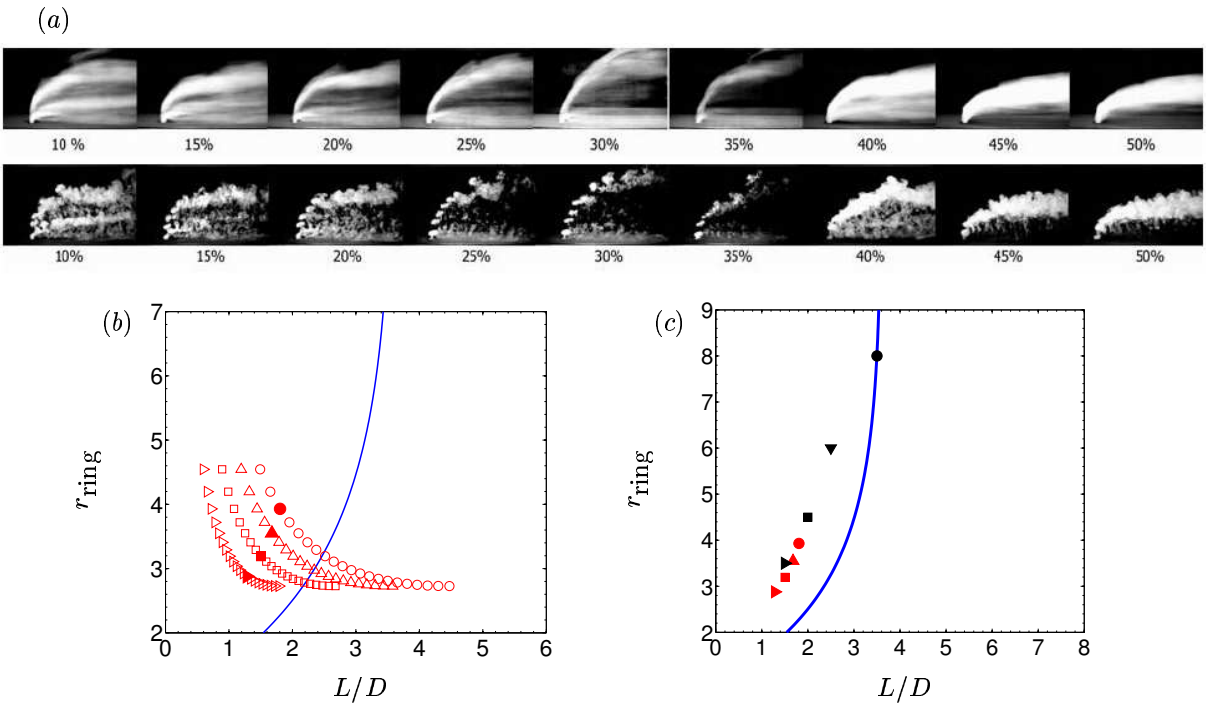

Figure 8. (a) Figure 4 from experiment of Shapiro *et al.* (2006), reprinted by permission; mean and instantaneous flow–field (case 1, $U'_{j,\mathbf{rms}} = 1.5$ m/s) with forcing frequency $f = 110$ Hz for duty cycle ranging from 10% to 50%. Maximum jet penetration occurs at 30% duty cycle corresponds to optimal pulse width ($\tau = 3$ ms). (b) The experimental conditions for varying pulse width or duty cycle are transformed in classification map for four frequencies: ○, 44 Hz; △, 55 Hz; □, 73.5 Hz; ▷, 110 Hz. As the pulse width increases for fixed $U'_{j,\mathbf{rms}}$, L/D increases and $r_{\mathbf{ring}}$ decreases. The filled symbols show the optimal conditions ($\tau = 3$ ms) at corresponding frequencies. The solid line denotes the transition curve. (c) Optimal conditions from experiments are compared along with simulatons. Red and black symbols correspond to experiment and simulations respectively.

Shapiro *et al.* (2006) performed controlled experiments of pulsed jets in crossflow. They note that specific values of pulse widths for a variety of forcing frequencies, produce distinct deeply penetrating vortex rings and under these conditions the jet penetration is maximum. They also note that these optimal conditions for penetration result in strongly bifurcating jets. Experiments are performed for 4 different combination of jets and crossflow combination at two different velocity ratios 2.58 and 4.0. The table 2 lists their experimental conditions for two cases denoted by 1 and 4 with jet velocity ratios 2.58 and 4.0 respectively. For each of these cases, optimal pulse width is being examined at a given frequency of square–wave jet excitation. For example, pulse width is varied at fixed frequency of 44 Hz for case 1 to find optimal pulse width. In each case, the excitation waveform matches $U'_{j,\text{rms}}$ as specified in table 2. Now, for each case, the equivalent stroke ratio and ring–velocity ratio can be computed from the given experimental conditions and can be mapped onto the classification map.

Figure 8(a) shows mean and instantaneous flow field of pulsed jets at 110 Hz as the duty cycle ranges from 10% to 50% in one of their experiment (case 1). The optimal penetration is obtained at duty cycle of 30% with pulse width of 3 ms. In fact, the optimal pulse widths at other frequencies (44, 55, 73.5 Hz) are found to be the same at 3 ms. Now, as the duty cycle or pulse width increases for fixed $U'_{j,\text{rms}} = 1.5$ m/s, the equivalent stroke ratio and ring-velocity ratio vary as shown in figure 8(b)–(c) for case 1 of their experiment. The stroke ratios and ring velocity ratios are computed using the peak–to–peak velocity difference. Figure 8(b) shows four sets of data corresponding to four different frequencies (44, 55, 73.5 and 110 Hz for case 1) denoted by different symbols. Note that at a given frequency, as the pulse width increases, stroke ratio

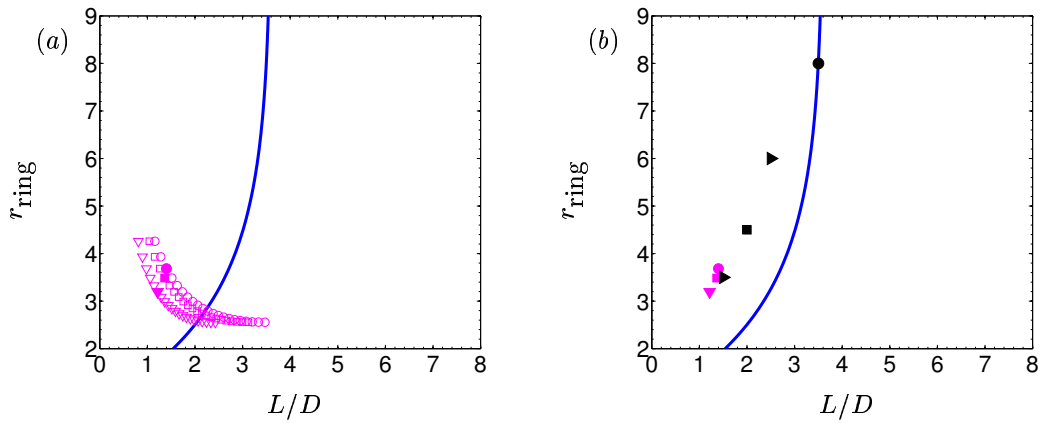

Figure 9. (a) Experimental conditions (case 4 of Shapiro *et al.*, $U'_{j,\mathbf{rms}} = 2.3$ m/s) with varying pulse width for different frequencies: ∘, 87 Hz; □, 96.7 Hz; ▽, 124.3 Hz, are mapped in stroke ratio and ring velocity ratio space. Filled symbols show the optimal conditions with pulse width 1.6 ms. Solid line denotes the transition curve. (b) Optimal condition for the experiment is compared with simulations. Pink and black symbols correspond to experiment and simulations respectively.

Table 4. Case 4 of Shapiro *et al.*; Optimal conditions ($U'_{j,\mathbf{rms}}$ is matched at 2.3 m/s).

Frequency Hz	Optimal τ	Optimal ring parameters equivalent L/D^*	r_{ring}
87	1.6 ms	1.40	3.68
96.7		1.34	3.53
124.3		1.21	3.19

increases and ring velocity ratio decreases. The optimal pulse width of 3 ms for each of these frequencies are denoted by solid symbols. The optimal stroke ratios and ring velocity ratios are also listed in table 3. Note that the optimal conditions lie on the left of the transition curve and decrease with ring velocity ratio as shown in figure 8(b). In figure 8(c), these optimal conditions in the experiments (case 1) are compared to optimal simulation data. Note that reasonable agreement of simulation data with the experiment is found and the experimental optimal conditions follow the same trend as observed in the simulations.

Similarly, in case 4 of Shapiro *et al.*'s experiment, optimal pulse width is examined at different frequencies. The experimental conditions for this case is listed in table 2. The pulse width is varied at a given frequency to match $U'_{j,\text{rms}} = 2.3$ m/s. In this case, the optimal pulse width is found at 1.6 ms at different frequencies. Figure 9(b) marks the experimental conditions in stroke ratio and ring velocity ratio space for three frequencies (87, 96.7 and 124.3 Hz) as the pulse width is varied. Note that as the pulse width increases, stroke ratio increases and ring velocity ratio decreases. The optimal conditions are listed in table 4 and marked in solid symbols in figure 9(b). In figure 9(c), these optimal experimental conditions are compared to simulation results. Note that reasonable agreement is obtained here.

In order to evaluate the concept of optimal L/D, Shapiro *et al.* (2006) also performed experiments by matching peak–to–peak jet velocity excitation amplitude ΔU_j. Experimental case 1 is performed by matching ΔU_j to observe the critical pulse width for optimal vortex formation and deeply penetrating jets. Optimal duty cycle for three different frequencies (55, 73.5 and 85 Hz) are reported as listed in table 5. The equivalent optimal ring parameters corresponding to the optimal duty cycle are also tabulated. For each

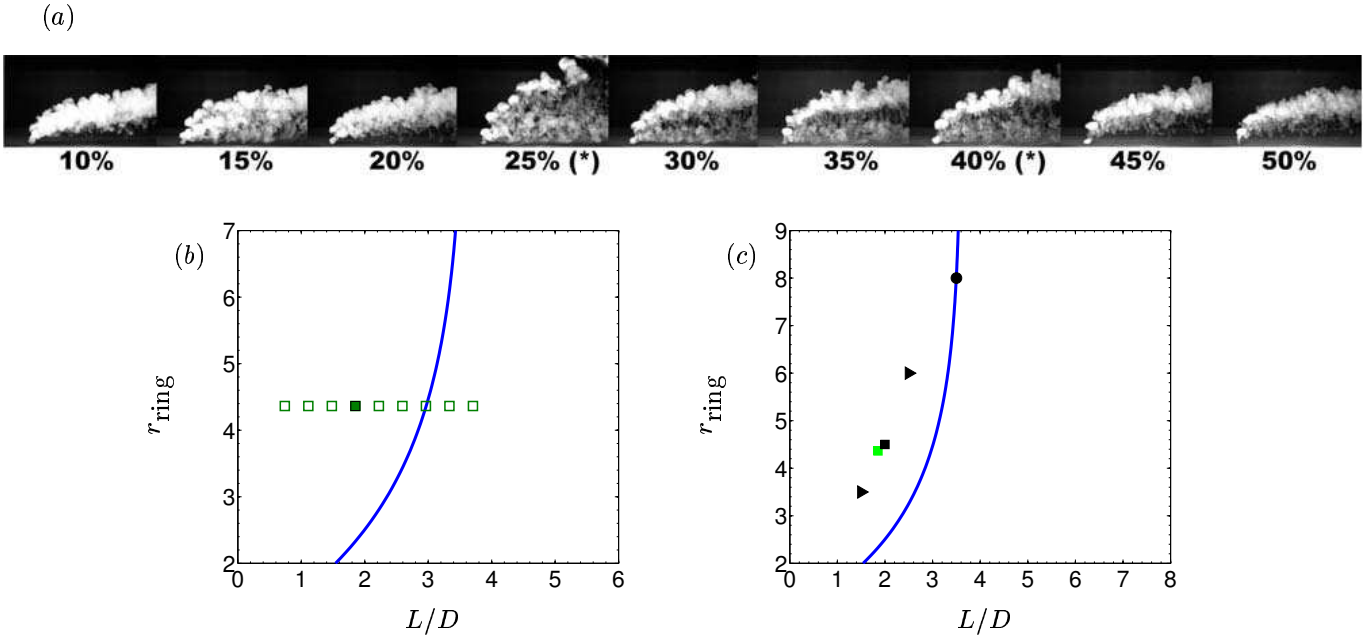

Figure 10. (a) Figure 6c from experiment of Shapiro *et al.* (2006), reprinted by permission; smoke visualization for experimental case 1, with peak–to–peak ΔU_j fixed at 4.8 m/s with forcing frequency $f = 85$ Hz for duty cycle ranging from 10% to 50%. Maximum jet penetration occurs at 25% duty cycle. (b) Experimental conditions are plotted in stroke ratio and ring velocity ratio co-ordinates. Filled symbol shows the optimal condition with duty cycle 25%. (c) Optimal condition for the experiment is compared with simulations.

Table 5. Case 1 Shapiro *et al.*; Optimal condition (ΔU_j is matched at 4.8 m/s)

Frequency Hz	Optimal α	Optimal ring parameters equivalent L/D^*	r_{ring}
55	15%	1.718	4.36
73.5	20%	1.714	
85	25%	1.852	

frequency, the L/D range of 1.7–2.0 is reported for optimal penetration. Interestingly, another L/D range of 3.2–4.2 is reported along with 1.7–2.0 for best vortical structures for lower frequencies. Figure 10(a) shows the instantaneous flow field for different duty cycle (10% to 50%) at 85 Hz. Note that th optimal penetration is achieved at duty cycle of 25%. The experimental conditions for this case at 85 Hz are transformed in stroke ratio and ring–velocity ratio space as shown in figure 10(b). As the duty cycle is increases, stroke ratio increases while ring–velocity ratio is fixed at 4.36. The optimal duty cycle of 25% corresponds to the L/D of 1.8 at $r_{\text{ring}} = 4.36$ (solid symbol in figure 10b). The optimal condition is plotted along with the simulation results in figure 10(c). Note that good agreement is obtained. The optimal condition at other frequencies are listed in table 5.

V. Conclusion

Controlled simulations of fully modulated laminar pulsed jets in crossflow are performed for a variety of jet and crossflow combinations at different velocity ratios with square–wave excitation. Optimal pulsing

conditions for maximum jet penetration into the crossflow are obtained for all the combinations examined. The evolution of pulsed jets in crossflow is explained on the basis of behavior of single vortex ring in the presence of crossflow. Sau & Mahesh (2008) developed a classification map (figure 1) for single vortex ring in crossflow. The classification map suggests that three different structures exist depending on ring parameters namely, stroke ratio and ring velocity ratio. The pulsing conditions can be transformed into the ring parameters and the flow field can be interpreted using the classification map. It is shown that the optimal conditions for pulsed jets can be predicted using the classification map.

Simulations suggest that optimal stroke ratios for pulsed jet penetration, decrease as the ring velocity ratio decreases. For high ring velocity ratios in pulsed jet simulations, optimal stroke ratio for penetration is almost equal to transition stroke ratio. However for lower velocity ratios, optimal stroke ratios are found to follow the transition curve and lie on the left of the curve. At a particular ring velocity ratio, the optimal stroke ratios are found in the regime close to the transition stroke ratio where upstream tilted single vortex ring is formed without any trailing column. These upstream tilted single rings penetrate deeper into the crossflow and a second stream of jet is formed near the wall due to the wake of these rings. In the case of single vortex ring in crossflow, the transition stroke ratio decreases with ring velocity ratio. Similarly, the optimal stroke ratio in pulsed jet decreases as the ring velocity ratio decreases. The rings generated for stroke ratios close to the transition curve, tend to interact even in the near field at lower velocity ratio. Thus, optimal stroke ratios are found to decrease faster than transition stroke ratio with ring velocity ratio. Duty cycle is another independent parameter which basically controls the spacing between the rings. For very high values of duty cycle, the rings interact in the very near field irrespective of the stroke ratio and no optimal is found. As long as the duty cycle is low, optimal penetration is found and optimal stroke ratio does not change as duty cycles changes.

So, for optimal penetration in pulsed jets, the forcing parameters should be such that the corresponding ring parameters, equivalent stroke ratio and ring velocity ratio, should follow the optimal curve predicted in the classification map using the simulations as shown in figure 6. Experiments of Shapiro *et al.* (2006) on pulsed jets in crossflow are interpreted using the ring parameters. The optimal conditions in those experiments are shown to agree very well with simulations data. It is shown that there is enough experimental evidence to support the ideas presented here using the simulation data. We propose therefore that the optimal map (figure 6) for pulsed jet in crossflows that can be used to obtain an *a-priori* estimate of optimal conditions.

VI. Acknowledgments

This work was supported by the Air Force Office of Scientific Research (AFOSR) under grant FA-9550-04-1-0064. Computer time was provided by the National Center for Supercomputing Applications (NCSA), Minnesota Supercomputing Institute (MSI) and the San Diego Supercomputer Center (SDSC).

References

[1]Blossey, P., Narayanan, S. & Bewley, T.R., 2001, Dynamics and control of a jet in crossflow: direct numerical simulation and experiments. *Proc. IUTAM Symp. Turbulent Mixing Combustion*, ed. A. Pollard & S. Candel, Kluwer Academic, Dordrecht, pp. 45–56.

[2]Chang, Y.K. & Vakili, A.D., 1995, Dynamics of vortex rings in crossflow. *Physics of Fluids*, **7(7)**, 1583–1597.

[3]Eroglu, A. & Briedenthal, R.E., 2001, Structure, penetration and mixing of pulsed jets in crossflow. *AIAA J.*, **39(3):** 417–423.

[4]Gharib, M., Rambod, E. & Shariff, K., 1998, A universal time scale for vortex ring formation. *J. Fluid Mech.*, **360:** 121–140.

[5]Hermanson J. C., Wahba A. & Johari H. 1998, Duty cycle effects on penetration of fully modulated, turbulent jets in crossflow, *AIAA J.* **36(10):** 1935–1937.

[6]Johari, H., Pacheco–Tougas, M. & Hermanson, J.C., 1999, Penetration and mixing of fully modulated jets in crossflow, *AIAA J.*, **37(7):** 842–850.

[7]Johari, H. 2006 Scaling of fully pulsed jets in crossflow. *AIAA J.* **44(11):** 2719-2725.

[8]Karagozian, A.R., Cortelezi, L. & Soldati, A., 2003, Manipulation and control of jets in crossflow, CISM Courses and Lectures No. 439, International Center for Mechanical Sciences, Springer Wien, New York.

[9]Mahesh, K., Constantinescu, G. & Moin, P., 2004 A numerical method for large–eddy simulation in complex geometries. *J. Comput. Phys.* **197:**, 215–240.

[10]M'Closkey, R.T., King, J.M., Cortelezzi, L. & Karagozian, A.R., 2002, The actively controlled jet in crossflow. *J. Fluid Mech.*, **452:** 325–335.

[11]Sau, R. & Mahesh, K. 2007, Passive scalar mixing in vortex rings. *J. Fluid Mech.* **582**, 449–491.

[12]Sau, R. & Mahesh, K. 2008, Dynamics and mixing of vortex rings in crossflow. *J. Fluid Mech.* **604**, 389–409.

[13]Shapiro, S.R., King, J.M., Karagozian, A.R. & M'Closkey, R.T., 2003, Optimization of controlled jets in crossflow, *AIAA Paper* 2003–634.

[14]Shapiro, S.R., King, J.M., Karagozian, A.R. & M'Closkey, R.T. 2006 Optimization of controlled jets in crossflow. *AIAA J.* **44**, 1292-1298.

[15]Wu, J.M., Vakili, A.D. & Yu, F.M., 1988, Investigation of the interacting flow of non-symmetric jets in crossflow, *AIAA J.*, **26(8):** 940–947.